Catalysis Science & Technology

ROYAL SOCIETY OF CHEMISTRY

PAPER

View Article Online
View Journal | View Issue

Cite this: *Catal. Sci. Technol.*, 2021, 11, 2762

Production of renewable oleo-furan surfactants by cross-ketonization of biomass-derived furoic acid and fatty acids†

Hannah Nguyen,[a] Yunzhu Wang,[b] David Moglia,[a] Jiayi Fu,[ab] Weiqing Zheng,[b] Marat Orazov*[ab] and Dionisios G. Vlachos*[ab]

Received 6th December 2020,
Accepted 22nd February 2021

DOI: 10.1039/d0cy02349c

rsc.li/catalysis

Synthesis of 2-dodecanoyl furan is a crucial step in the formulation of oleo-furan sulfonates as bio-surfactants from biomass-derived furans and vegetable-oil-derived molecules. Herein, cross-ketonization of 2-furoic acid and lauric acid is proposed to produce the bio-surfactant precursor. Among the commonly reported metal oxide ketonization catalysts, the inexpensive and abundant iron oxides are demonstrated as effective and recyclable catalysts, enabling up to 77% selectivity to 2-dodecanoyl furan at 56% lauric acid conversion. Catalyst characterization by X-ray diffraction, H_2 temperature-programmed reduction, and X-ray photoelectron spectroscopy indicates that Fe_3O_4 is the catalytically active and stable phase. ^{13}C isotopic tracing experiments suggest that cross-ketonization on Fe_3O_4 proceeds *via* a β-keto acid intermediate.

Introduction

Recent research in biomass conversion has significantly advanced the science and technology of converting the most naturally abundant renewable source of carbon to chemicals. Specifically, the non-edible biomass-derived furans can be upgraded to valuable chemicals, such as plastics, rubber, lubricants, and detergents.[1–7] Examples include the synthesis of *para*-xylene *via* cycloaddition of dimethyl furan and ethylene,[1] butadiene *via* "dehydra-decyclization" of tetrahydrofuran,[4] C_{33-45} base-oil lubricants,[5] and oleo-furan sulfonates (OFSs), which possess excellent detergency. The structure of OFSs (shown in Fig. 1) includes a central furan moiety that links a hydrophobic hydrocarbon chain to a hydrophilic sulfonate. Park *et al.* evaluated the surfactant properties of OFSs using the critical micelle concentration (CMC), defined as the minimum surfactant concentration for micelle formation, the Kraft point (T_{Kraft}), below which surfactants form solid crystals, and their stability in hard water.[7] OFSs with linear alkyl chains exhibit enhanced surfactant performance as evidenced by their lower CMC and T_{Kraft} than petroleum-derived alkylbenzene sulfonates (LAS). The furan moiety improves surfactant's solubility compared to the benzene moiety. Moreover, the OFS function in hard water, *i.e.*, in the presence of Ca^{2+}, is much better than the LAS's. Overall, OFSs enable the (1) utilization of renewable lignocellulosic feedstock, (2) enhanced detergency in cold water applications, and (3) improved stability in hard water, eliminating the need for costly chelating agents used in conventional LAS.

The OFSs preparation involves the formation of a 2-alkoylfuran intermediate *via* Friedel–Crafts acylation of furan with a vegetable-oil-derived, long-chain (C_8–C_{18}) carboxylic acid or fatty acid anhydride. Optionally, hydrodeoxygenation of the ketone group may be used to increase the hydrophobicity of the alkyl chain. Finally, sulfonation introduces the hydrophilic head of the surfactant. Among these steps, the C–C coupling reaction to form 2-alkoylfuran is a bottleneck. In one route, furan is coupled with a fatty acid anhydride (*e.g.*, lauric acid C_{12} anhydride) over Al-SPP, a hierarchical porous Brønsted acid zeolite, to yield up to 90% of the acylated furan (Fig. 1, pathway A). Though selective, this pathway produces an equimolar amount of lauric acid, with a high boiling point

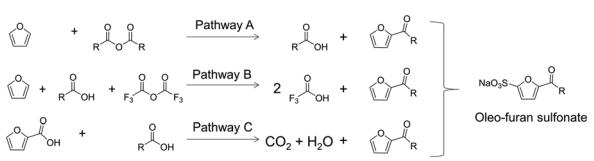

Fig. 1 Pathways to produce oleo-furan sulfonate bio-surfactant. R represents the *n*-$C_{11}H_{23}$ chain; other chains could also be considered. Path C is the one developed herein.

[a] *Department of Chemical and Biomolecular Engineering, University of Delaware, Newark, Delaware 19716, USA. E-mail: orazov@udel.edu, vlachos@udel.edu*
[b] *Catalysis Center for Energy Innovation, Newark, Delaware 19716, USA*

† Electronic supplementary information (ESI) available. See DOI: 10.1039/d0cy02349c

(~298 °C), rendering its separation and recycling difficult. An alternative route utilizes trifluoroacetic anhydride to convert lauric acid to lauric–trifluoroacetic anhydride, which then acylates the furan (Fig. 1, pathway B). This pathway generates a waste stream of corrosive trifluoroacetic acid.[7] While direct Friedel–Crafts acylation using acids and furan is highly desirable, thermodynamic calculations show that the chemistry is equilibrium limited for long chains, resulting in low yields (see ESI† for equilibrium estimations).

Due to the disadvantages of the current approaches, herein, we propose a new synthesis of 2-alkoyl furan *via* cross-ketonization of 2-furoic acid and lauric acid using heterogeneous catalysts (Fig. 1, pathway C). The cross-ketonization strategy offers ease of separation and recyclability of solid catalysts and produces only water and carbon dioxide as byproducts. It also does not suffer from the equilibrium limitations of acylation (see ESI† for equilibrium estimations).

Ketonization is an established C–C coupling reaction to prepare symmetrical dialkyl ketones or cyclic ketones from aliphatic acids or diacids, respectively. Common examples include the ketonization of acetic acid to acetone[8,9] and adipic acid cyclization to cyclopentanone.[9] Two different carboxylic acids lead to self- and cross-ketonization, with the former reducing the selectivity to the desired cross-ketonization product.[10–12] Early work on ketonization of acetic acid was facilitated by alkali and alkaline earth oxides *via* decomposition of the acetate salts, which forms *via* the reaction of the acid with the bulk oxides.[13,14] Recent catalyst developments show that ketonization occurs on the surface of zeolites and high-lattice-energy metal oxides, such as TiO_2, ZrO_2, CeO_2, their mixed oxides, and transition metal (*e.g.*, Pd, Ru, Co)-doped oxides.[15–19] Catalyst properties that may affect ketonization activity include, but are not limited to, redox, acid–base properties, and interaction of the carboxylic acid with the oxide surface. Comprehensive reviews on the catalysis and ketonization mechanism of short-chain carboxylic acids have been reported elsewhere.[20,21] Extensive mechanistic research has shown that α-hydrogen (α-H) in at least one of the carboxylic acid molecules is critical for the surface reaction to take place.[15,22] The reaction rate increases monotonically with the number of α-H atoms in the absence of steric hindrance. For instance, the self-ketonization of propionic acid (with two α-H) occurs ten times faster than 2-methyl propionic acid (with one α-H).[10] Accordingly, one may expect a slower reaction rate for cross-ketonization since 2-furoic acid does not contain an α-H. While most prior ketonization studies focused on small gas-phase molecules, the high boiling point of lauric acid requires a liquid reaction. Therefore, the proposed cross-ketonization chemistry entails challenges, namely (1) slow rate of cross-ketonization, (2) lack of mechanistic insights, and (3) limited related literature. This report demonstrates the selective production of 2-dodecanoyl furan bio-surfactant precursor from biomass-derived 2-furoic acid and vegetable-oil-derived lauric acid, using earth-abundant metal oxide catalysts. The reaction mechanism and catalyst active sites are elucidated to guide further research on catalyst design.

Experimental section

Materials

2-Furoic acid and *n*-dodecanoic (lauric) acid were purchased from Sigma Aldrich. Solvents *n*-dodecane, cyclohexane, and dimethyl sulfoxide (DMSO) were acquired from Fisher Scientifics. The metal oxides, including iron(II) oxide (FeO), iron(III) oxide (Fe_2O_3), and iron(II,III) oxide (Fe_3O_4), titanium oxide (TiO_2), zirconium oxide (ZrO_2), gamma aluminum oxide (γ-Al_2O_3), and cerium oxide (CeO_2) were obtained from Sigma Aldrich. All chemicals were used as received.

Catalytic reaction and analysis

Reactions were carried out in a 100 mL Parr reactor vessel, with a glass liner, containing 30 mL of *n*-dodecane solvent, 2-furoic acid and lauric acid as reactants, 0.2 g metal oxide catalyst, under 20 bar N_2 pressure, with lauric acid as the limiting reagent. *N*-Dodecane was chosen as the solvent due to its inertness, low vapor pressure, and the ability to solubilize lauric acid and the desired product, 2-dodecanoyl furan. The reactor was heated up to the desired temperature in a fitted band heater, using an inhouse made PID controller, on a magnetic stir bar. After a designated time, the reactor was quenched in an ice bath to stop the reaction. Due to its low solubility in *n*-dodecane at room temperature, 2-furoic acid was extracted from the post-reaction solution by DMSO for further quantification. The samples were then filtered for further analysis. In recyclability experiments, the spent catalysts were collected, washed with cyclohexane, which can dissolve dodecane and quickly evaporate in air, and air-dried at room temperature overnight before used for the next catalytic experiment. Due to the 10–15% typical loss of spent catalysts during filtering, washing, and handling, three repeated experiments (run 1) were conducted with a fresh catalyst to collect enough spent catalysts for the second recycle (run 2), and two repeated experiments were conducted for run 2 to collect enough spent catalysts for the third recycle (run 3). Products were identified and quantified with a gas chromatogram-mass spectrometer (GC-MS) system (Agilent 7890B) and with a gas chromatogram-flame ionization detector (GC-FID) instrument, respectively. Both the GC-MS and GC-FID were equipped with an HP-1 column (Agilent). When available, calibration curves from commercial standards were used to quantify the concentrations of reactants and products. Because a commercial standard of 2-dodecanoyl furan was unavailable, this product was quantified using the effective carbon number (ECN) method.[23] The ECN of 2-dodecanoyl furan was determined from the ECN of the commercially available 2-acetyl furan and hexane. The method was verified with the agreement between experimentally measured and calculated calibration slope for 2-hexanoyl furan (see Fig. S1 and Table S1†).

Catalyst characterization

Surface area and porosity were determined from N_2 physisorption data at 77 K using the Micromeritics ASAP 2020 instrument. The crystallinity of the fresh and spent catalysts were measured by a Bruker D8 X-ray diffraction (XRD) instrument equipped with a monochromatic Cu $K\alpha_1$ line (λ = 0.154 nm) at 40 kV and 40 mA, operating in 2θ range of 5–80° at a scanning rate of 0.02° s^{-1}. Temperature programmed reduction (TPR) by hydrogen was performed on a thermogravimetric analysis (TGA) instrument (TA Q600 HT) using 50 mL min^{-1} of 5% H_2 in N_2 as the flowing gas in the 25–1200 °C temperature range. In addition, H_2-TPR was also conducted in a downward flow reactor. X-ray photoelectron spectra (XPS) of the catalysts were collected on a Thermo-Fisher K-alpha XPS, equipped with Al-Kα X-ray monochromatic source with 400 μm spot size. The spent catalysts were handled in an air-free glovebox and transferred to a vacuum transfer module (Thermo Scientific) before XPS measurements to eliminate air exposure. Iron species concentration in the post-reaction filtrates was measured by ICP. One milliliter of the filtrate was heated in a vacuum oven at 200 °C to evaporate the dodecane. The remaining solids were dissolved in a 20 mL mixture containing 50 v/v% ethanol, 2.5 v/v% HNO_3 and 47.5 v/v% water, and sonicated in a 50 °C water bath for 30 min. The mixture was further diluted 50 times using a 5 v/v% HNO_3 solution for ICP analysis. Six standards containing 1 ppb, 10 ppb, 50 ppb, 100 ppb, 500 ppb, and 1000 ppb of Fe (SPEX CertiPrep) were used for calibration. The Fe content in each sample was measured using a Thermo Scientific iCAP triple quad-inductively coupled plasma-mass spectrometer (TQ-ICP-MS). The results were averaged from triplicates. ^{45}Sc (VHG Lab product # LIS2-100) was used as an internal standard to monitor the machine drift throughout the measurement. ^{45}Sc was used due to its m/z ratio close to the target element Fe and was presumably not present in the samples. Results with recovery rates between 80 to 120% were considered valid.

Results and discussion

The catalytic activity of metal oxides for cross-ketonization of 2-furoic acid and lauric acid

We screened various commercial metal oxides with high lattice energies, which are active for surface-catalyzed ketonization,[8,15,24,25] for the reaction of 2-furoic acid and lauric acid in dodecane at 300 °C (Fig. S2†) and 316 °C (Fig. 2), with the molar ratio of 5 (see ESI† for tests at other 2-furoic acid to lauric acid molar ratios (Fig. S3†), and test for external mass transfer limitations in Fig. S4†).

GC-detected products included long-chain ketones, 2-dodecanoyl furan (desired product), and 12-tricosanone, resulting from the cross- and self-ketonization of the lauric acid, respectively, and furan, from the decarboxylation of 2-furoic acid, as proposed in Fig. 3. While the furan yield, based on 2-furoic acid, was >30% on all catalysts, ketones only formed over iron oxides (Fe_xO_y), ceria, and titania after

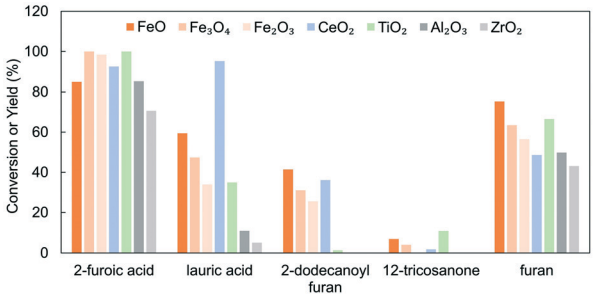

Fig. 2 Performance of various commercial metal oxides in the reaction of 2-furoic acid with lauric acid in *n*-dodecane. Reaction conditions: 0.05 M lauric acid, 0.25 M 2-furoic acid, 0.2 g catalyst, 316 °C, 90 min, 20 bar N_2, 800 rpm. Pressure at reaction temperature = 47 bar.

90 min. Among these, the highest selectivity (up to 77% at 316 °C and 84% at 300 °C) to the cross-ketonization product, based on the lauric acid conversion and 2-dodecanoyl yield, was on iron oxides (Fe_xO_y). This demonstrates the feasibility of cross-ketonization for the oleo-furan sulfonate production. However, the 2-dodecanoyl furan yield is still lower than the 90% yield of the pathway A.[7] The yield to 2-dodecanoyl over iron oxides for three consecutive cycles at 316 °C (Fig. 4) was within experimental error. These recyclability experiments were conducted at near to full conversion of furoic acid to assess yields. A detailed catalyst stability/deactivation study in future work should be carried out at low conversions.

The post-reaction solutions were yellowish, and the total GC carbon balance for 2-furoic acid was lower than 80%, indicating the formation of organic deposits (see Fig. S5† for carbon balance analysis). Di-furfuryl ketone was not detected from 2-furoic acid self-ketonization, consistent with the critical role of α-H in the ketonization and the fact that the reaction takes place on the catalyst surface instead of in the bulk, using alkali, alkaline earth, and rare earth metal oxides,[13,20] where an α-H is not required.

Interestingly, the filtered solutions from the FeO-catalyzed reactions turned reddish upon exposure to air, and iron species were determined with ICP analysis (Table S2†). After removing the spent FeO particles in the first cycle by filtration, fresh 2-furoic acid and lauric acid were added to the iron-containing filtrate solution, and the mixture was brought to reaction conditions. 2-Dodecanoyl furan formed

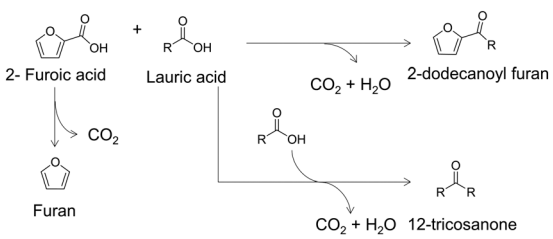

Fig. 3 Proposed reaction network for the reaction of 2-furoic acid and lauric acid in *n*-dodecane by iron oxide catalyst. Only paths to detectable products are shown. R represents the *n*-$C_{11}H_{23}$ group. Other chains could also be used.

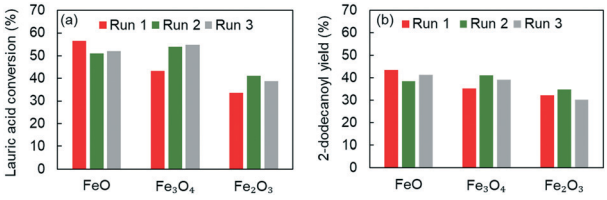

Fig. 4 Lauric acid conversion (a) and 2-dodecanoyl furan yield (b) in dodecane for three consecutive uses of the catalyst. Reaction conditions: 0.05 M lauric acid, 0.25 M 2-furoic acid, 0.2 g catalyst, 316 °C, 90 min, 20 bar N_2, 800 rpm. Pressure at reaction temperature = 47 bar.

at 15% yield (Fig. S6†), suggesting that homogeneous iron species (likely carboxylate complexes), created during the reaction over FeO, are active for cross-ketonization. No homogeneous iron species were detected in Fe_2O_3 and Fe_3O_4; their post-reaction filtrates exhibited no activity. CeO_2 is promising but gives higher carbon loss of lauric acid (Fig. S5†). Given their promising performance at the test conditions, the commercial iron oxides were down-selected to provide further insights into the cross-ketonization of fatty acids and furoic acid.

Determination of catalyst active centers

The BET surface area and pore volumes of the fresh iron oxides increased in the order of FeO < Fe_3O_4 < Fe_2O_3 and were overall the lowest (<35 m^2 g^{-1} and <0.08 cm^3 g^{-1}) among the screened catalysts, indicating that the materials are almost nonporous and the catalytic reactions take place mostly on their external surfaces (Table S3†). After the third reaction cycle, the surface area and pore volume substantially increased, remained unchanged, and decreased for FeO, Fe_3O_4, and Fe_2O_3, respectively. The unexpected enhancement of surface area by more than 2-orders of FeO indicated a significant alteration in the catalyst morphology. XRD patterns of the fresh iron oxides displayed their expected polymorphs (Fig. 5). The XRD patterns of γ-Fe_2O_3 (maghemite) in the tetragonal structure and Fe_3O_4 (magnetite) are not distinguishable because both oxides have the inverse spinel-type structure.[26] However, some maghemites contain other cations in the octahedral Fe vacancies,[27] giving additional XRD peaks in the fresh commercial Fe_2O_3 of this work (matched with maghemite-Q-00-02501402). After the reaction, the spectrum of Fe_3O_4 remained unchanged, the aforementioned additional XRD peaks in the spent Fe_2O_3 disappeared, and the diffraction pattern of the used FeO transformed to that of Fe_3O_4. In short, all Fe_xO_y catalysts displayed the crystallinity pattern of magnetite, suggesting reduction of Fe_2O_3 and oxidation of FeO during the reaction. The same phenomenon was reported for iron oxides supported on silica after acetic acid ketonization.[28] The drastic change in the iron oxides' surface area and porosity may be attributed to their corresponding oxidation state transformation.

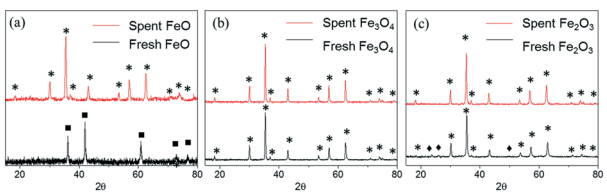

Fig. 5 XRD pattern of the fresh and spent iron oxides FeO (a), Fe_3O_4 (b), Fe_2O_3 (c) with assigned diffraction peaks for FeO (■), Fe_3O_4 or γ-Fe_2O_3 (*), and additional octahedral Fe cation peaks (♦).

To better understand the reduction of the Fe_xO_y, temperature-programmed reduction by H_2 coupled with thermogravimetric analysis were performed on the fresh iron oxides. Standard reduction of Fe_2O_3 was previously postulated to take place *via* a 3-step mechanism: Fe_2O_3 → Fe_3O_4 → FeO → Fe.[29] However, the TPR–TGA profiles of the commercial iron oxides indicate that the reduction is more complex and involves multiple convoluted steps, in agreement with other literature[30–32] (Fig. S7†). Specifically, partial reduction of Fe_2O_3 to Fe_3O_4 was observed in the 240–416 °C temperature range. Total reduction to Fe^0 metal occurred in the range of 416–743 °C. Fe_3O_4 reduction took place at 343–457 °C first, and complete reduction to Fe^0 occurs at 457–984 °C. The cross-ketonization reaction temperature is 316 °C is in the temperature range of Fe_2O_3 reduction to Fe_3O_4, as indeed observed by XRD. However, the reaction temperature is lower than the reduction temperature of Fe_3O_4, explaining the stability of the spent Fe_3O_4. Lastly, the reduction of FeO was minimal for temperatures lower than about 600 °C. It is well documented that FeO is thermally unstable at temperatures lower than 570 °C and the disproportionation reaction of FeO to Fe metal and Fe_3O_4 takes place in the temperature range of 250–600 °C without hydrogen consumption,[31] explaining the apparent oxidation of FeO to Fe_3O_4 during the ketonization reaction. The metallic Fe formed by disproportionation likely reacted with the acid reagents to generate homogeneous iron(II) carboxylates. These then oxidized to iron(III) to turn reddish after exposure to air and were active for cross-ketonization, as described above. Homogeneous iron species observed in the filtrate after the second and third runs of FeO indicate that the disproportionation was not complete during the reactions; some FeO nanoparticles under the detection limit of XRD (<5 nm) were still present in the spent FeO. Other iron(II) salts, *e.g.*, ferrocene (see Fig. S2†), are effective for cross-ketonization.

In addition to XRD and H_2 TPR–TGA techniques, we employed XPS to investigate the changes of the catalyst surfaces based on the binding energies of Fe 2p in fresh and spent catalysts (Fig. 6). Interestingly, the binding energy of Fe 2p photoelectrons of all the fresh iron oxide catalysts is the same at 711.0 eV for Fe $2p_{3/2}$ and 724.4 eV for Fe $2p_{1/2}$, corresponding to Fe^{3+} according to literature values.[33] The observed satellite peak at 719.4 eV, which is characteristic of Fe_2O_3, suggests the oxidation of the Fe on the surface of the

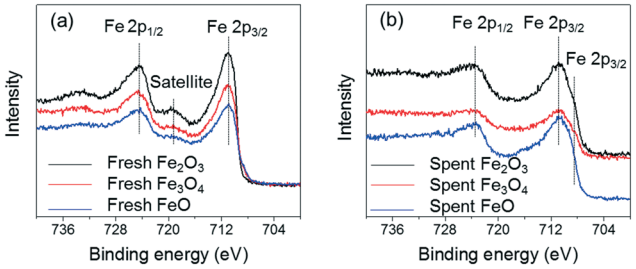

Fig. 6 XPS spectra of Fe 2p on the iron oxide catalyst surfaces (a) before and (b) after the cross-ketonization reaction.

commercial magnetite and wustite, probably due to extended exposure to air. After the reaction, clear shifts in Fe $2p_{3/2}$ peaks of the used catalysts to 710.6 eV are seen, a value in between Fe $2p_{3/2}$ binding energy of Fe_2O_3 (711.0 eV) and FeO (709.0 eV).

A shoulder at 709.0 eV, assigned to Fe $2p_3$ of FeO, was observed in all XPS spectra of the spent catalysts. Therefore, the catalyst surfaces of all Fe_xO_y catalysts were reduced from Fe^{3+} to a mixture of Fe^{3+} and Fe^{2+} post-reaction. The disappearance of the satellite peaks in the spent catalysts provides further support that the catalyst surfaces contain Fe_3O_4. Therefore, the initially oxidized catalyst surfaces of all iron oxide catalysts are reduced to Fe_3O_4 during the reaction, in agreement with the XRD results of the bulk FeO/Fe_2O_3. Interestingly, a closer look at the reaction evolution over Fe_3O_4 shows no 2-dodecanoyl furan production during the first 20 min of the reaction followed by rapid formation (Fig. S8†).

This induction period suggests that the initial Fe_2O_3 surface (as measured by XPS) transformed to the catalytically active form – potentially Fe_3O_4. To verify the hypothesis, we reduced the commercial Fe_3O_4 with H_2 at 316 °C for 30 min in the dodecane solvent before using it for the cross-ketonization reaction. The resulting material exhibited much higher activity, *i.e.*, 36% of 2-dodecanoyl furan yield (Fig. 7), whereas the starting material resulted in no measurable yield. The XPS spectrum of Fe 2p of the pre-reduced Fe_3O_4 is similar to that of the spent Fe_3O_4 after a standard reaction experiment (Fig. S9†). Specifically, the Fe $2p_{3/2}$ binding energy shifted to a lower value of 710.6 eV, with a shoulder at 709 eV, assigned to Fe^{2+} $2p_{3/2}$. The absence of a satellite peak confirmed the generation of Fe_3O_4 on the surface. The enhancement of Fe_3O_4 catalytic activity after H_2 pretreatment indicates that the newly formed Fe^{2+} centers on the catalyst surface are responsible for cross-ketonization. The improvement in the ketonization activity of Fe_2O_3 in the presence of H_2 has been reported for acetic acid ketonization.[34,35] We hypothesize that even though the standard reaction conditions were under inert N_2, either the reagents, intermediates, or the solvent in Fig. 3 act as reducing agents during the induction time, thereby reducing the Fe^{3+} centers to generate a catalytically active surface for ketonization. To better understand this finding, further experiments were conducted. When the catalysts were pretreated with a dodecane solution of 2-furoic acid or lauric acid individually at 316 °C for 30 min prior to the catalytic reaction, similar enhancements in catalytic activity were observed at 20 min (Fig. 7).

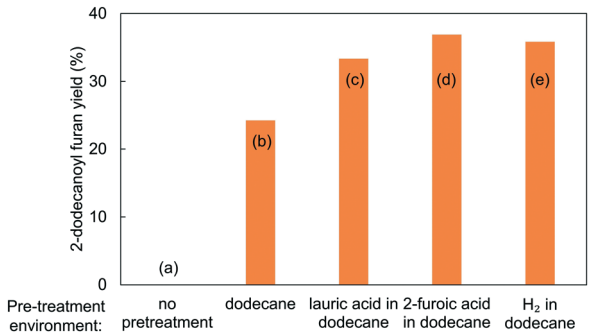

Fig. 7 Cross ketonization activity of Fe_3O_4 catalysts exposed to different pretreatment conditions: (a) catalyst as received; catalyst pretreated in a dodecane solution of (b) pure dodecane, (c) 0.05 M lauric acid, (d) 0.25 M 2-furoic acid, and (e) 5 bar of H_2. Pretreatment conditions: 316 °C, 30 min, 0.2 g fresh Fe_3O_4. Reaction conditions: 0.05 M lauric acid, 0.25 M 2-furoic acid, 316 °C, 20 min, 20 bars of N_2, 0.2 g Fe_3O_4.

Interestingly, an increased 2-dodecanoyl furan yield was also noted when the catalyst was pretreated in dodecane solvent alone, although the effect was not as pronounced as in the cases of using lauric acid, 2-furoic acid, or H_2 gas. XPS measurements of all the pretreated Fe_3O_4 catalysts displayed the Fe 2p spectra of Fe_3O_4 instead of the oxidized surface of the fresh magnetite (Fig. S9†). After pretreating the catalyst in dodecane at reaction conditions, traces of 2, 3, and 5-dodecanone were detected in GC-MS, suggesting oxidation of dodecane. We propose that the solvent dodecane is dehydrogenated and releases H_2 or surface species that reduce the catalyst surface. Lauric acid or 2-furoic acid in dodecane probably promotes the formation of reducing agents, such as H_2 and CO, *via* dehydrogenation/decarbonylation of the acid reactants. As a result, the cross-ketonization activity when the catalysts are pre-reduced with lauric acid or 2-furoic acid solution is higher than that with pure dodecane. Iron-based oxides are effective in dehydrogenation and oxidation,[29,36] corroborating this hypothesis. The detailed mechanism of reducing agent formation during the reaction is outside the scope of this work. H_2, CO, or CO_2, if formed, were not detected in GC-MS analysis, likely due to their trace concentration in the inert N_2 headspace. A schematic of the changes in the oxidation state of the Fe_3O_4 catalyst surface after pretreatment and reaction is shown in Fig. S10.† The enhanced catalytic-activity correlation with the catalyst surface reduction indicates that a reduced iron oxide surface facilitates ketonization, and Fe^{2+} is the likely catalytically active center.

In addition to the redox properties, the role of acidity of the metal oxides was evaluated using pyridine adsorption IR measurements on the catalysts (see Fig. S11 and ESI† for more details). The iron oxides exhibited little acidity while having the highest cross-ketonization activity. In contrast,

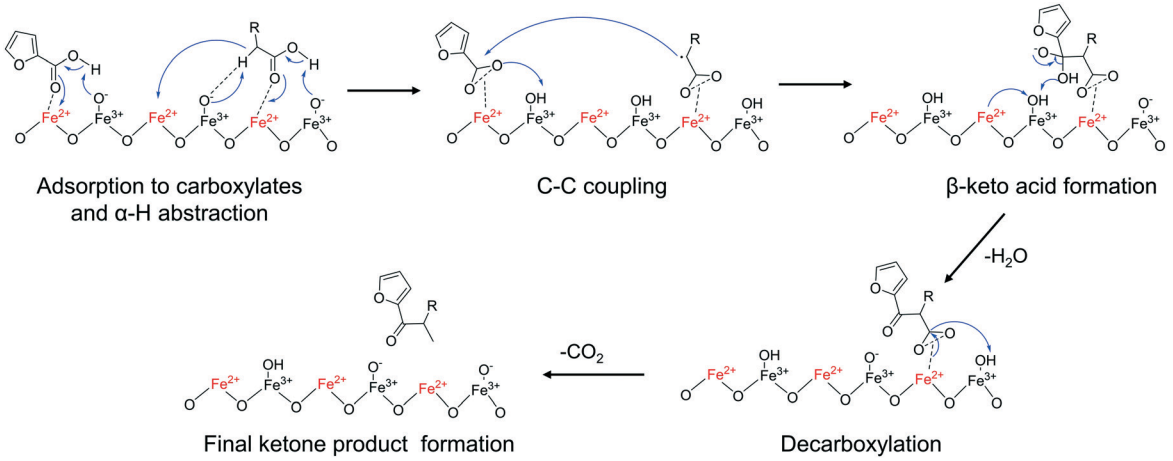

Fig. 8 Proposed reaction mechanism of cross-ketonization of 2-furoic acid and lauric acid on Fe_3O_4.

TiO_2 showed the highest acid density with no cross-ketonization activity. Therefore, we proposed that the catalyst acid density does not substantially affect the cross-ketonization rate under our conditions.

Reaction mechanism

Metal oxides facilitate surface-catalyzed ketonization *via* two possible mechanisms. A ketene ($R_2C{=}C{=}O$) forms *via* dehydration of the first carboxylic acid that contains an α-H, which then couples with the second adsorbed carboxylate to create the final ketone product.[25,37] Alternatively, other studies have provided evidence that a β-keto-acid, which has a ketone group at the β position of the carboxylic acid and can readily decarboxylate to form the ketone and CO_2, is the intermediate of ketonization.[10,22,38,39]

In the latter pathway, the α-H containing adsorbed carboxylate undergoes α-H abstraction by a surface metal site to form an anion radical, which attacks the adjacent second adsorbed carboxylate to give a β-ketoacid intermediate. Accordingly, the carbonyl group of the ketone product is inherited from the parent carboxylic acid of ketene in the ketene-like mechanism or from the second adsorbed carboxylate in the β-keto acid mechanism. Since only lauric acid contains an α-H, isotopically labeled lauric acid with ^{13}C at the C_1 position was employed to distinguish between the two reaction paths. GC-MS fragment patterns of the 12-tricosanone product show one unit shift to a higher *m*/*z* ratio (Fig. S12b†) compared to that in the unlabeled lauric acid (Fig. S12a†), suggesting a ^{13}C in the structure of self-ketonization of lauric acid. The GC-MS fragmentation of the cross-ketonization product and the standard 2-dodecanoyl furan are the same, indicating no ^{13}C incorporated into the 2-dodecanoyl furan; the carbonyl group arises from the 2-furoic acid (Fig. S.12c†). The results support the β-keto acid intermediate acid mechanism. Consequently, we postulate the catalytic pathway illustrated in Fig. 8. Accordingly, the surface Lewis acid Fe^{2+} sites facilitate the initial adsorption of 2-furoic acid and lauric acid to their corresponding surface carboxylates prior to the α-H abstraction from a basic oxygen site. C–C coupling between the adsorbed carboxylates generates the β-keto acid, thermally decomposing to the final product, 2-dodecanoyl furan. Coordinately unsaturated metal cations are necessary for surface carboxylate formation.[15,18,40] As the density of the surface Fe^{2+} increases, so does the probability of two adjacent carboxylates to form the β-keto acid. A similar reaction mechanism has been proposed for the vapor phase ketonization of propanoic acid to 3-pentanone over CeO_2–Mn_2O_3.[10] In addition, the roles of redox properties and surface oxygen vacancy on maintaining ketonization activity have been demonstrated for other metal oxides, such as CeO_2, ZrO_2, and TiO_2.[41,42] Numerous studies have utilized metal doping of metal oxides and/or catalyst pretreatment to create oxygen vacancies and unsaturated metal cations and by doing so to ultimately increase ketonization activity,[10,18,43] suggesting a potential strategy for improved activity in this system.

Conclusions

In this work, we introduced a method to produce oleo-furan surfactant precursors *via* cross-ketonization of biomass-derived furoic acid and vegetable-oil-derived lauric acid to 2-dodecanoyl furan. The volatile byproducts and solid catalysts can easily be separated from the desired product stream. In addition, one can use fatty acids instead of their anhydrides, without the typical thermodynamic limitations of the acylation reaction. This aspect is expected to minimize process waste.

Among the tested catalysts, earth-abundant, commercially-available iron oxides are active and selective towards cross-ketonization and were employed for further mechanistic studies. Detailed catalyst characterization, structure–activity relationships, and elucidation of reaction pathways provide insights into the active catalyst centers, reaction mechanism, and stability of the catalysts. XRD and XPS measurements of the fresh and spent catalysts reveal that the bulk and surface of all tested iron oxides transform to a stable Fe_3O_4 phase

during the reaction. Enhancement in the pre-reduced catalyst surface reactivity leads us to hypothesize that surface Fe^{2+} is critical for the reaction. ^{13}C isotopic labeling indicates that adjacently adsorbed laurate and furoate couple on the Fe^{2+} sites to form the corresponding β-ketoacid, which is then decarboxylated to 2-dodecanoyl furan. The iron oxide catalysts maintain activity for three consecutive cycles tested herein. The insights obtained here can guide future work on process and catalyst optimization for this new path to renewable surfactants.

Author contributions

Dionisios G. Vlachos: conceptualization, supervision, writing – review & editing; Marat Orazov: conceptualization, supervision, writing – review & editing; Hannah Nguyen: methodology, validation, investigation, data curation, writing – original draft; Yunzhu Wang: investigation, data curation; David Moglia: investigation, data curation; Jiayi Fu: investigation; Weiqing Zheng: methodology, validation.

Conflicts of interest

There are no conflicts to declare.

Acknowledgements

This work was supported as part of the Catalysis Center for Energy Innovation, an Energy Frontier Research Center funded by the US Dept. of Energy, Office of Science, Office of Basic Energy Sciences under award number DE-SC0001004. This research used Thermo Scientific iCAP TQ-ICP-MS in the Advanced Materials Characterization Lab (AMCL) at the University of Delaware. The authors want to acknowledge Chin-Chen Kuo for ICP measurements and suggestions on ICP sample preparations, Dr. Stavros Caratzoulas for assisting with the Gaussian calculations of the thermochemistry equilibrium, and Prof. Raul Lobo for useful discussions.

Notes and references

1 N. Nikbin, S. Feng, S. Caratzoulas and D. G. Vlachos, *J. Phys. Chem. C*, 2014, **118**, 24415–24424.
2 T. A. Brandvold, *US Pat.*, US20100331568A1, Honeywell UOP LLC, 2012.
3 M. Peters, J. Taylor, D. E. Henton, L. E. Manzer, *US Pat.*, EP2401307A1, Gevo Inc, 2012.
4 O. A. Abdelrahman, D. S. Park, K. P. Vinter, C. S. Spanjers, L. Ren, H. J. Cho, D. G. Vlachos, W. Fan, M. Tsapatsis and P. J. Dauenhauer, *ACS Sustainable Chem. Eng.*, 2017, **5**, 3732–3736.
5 M. Balakrishnan, E. R. Sacia, S. Sreekumar, G. Gunbas, A. A. Gokhale, C. D. Scown, F. D. Toste and A. T. Bell, *Proc. Natl. Acad. Sci. U. S. A.*, 2015, 201508274.
6 D. Jadhav, A. M. Grippo, S. Shylesh, A. A. Gokhale, J. Redshaw and A. T. Bell, *ChemSusChem*, 2017, **10**, 2527–2533.
7 D. S. Park, K. E. Joseph, M. Koehle, C. Krumm, L. Ren, J. N. Damen, M. H. Shete, H. S. Lee, X. Zuo and B. Lee, *ACS Cent. Sci.*, 2016, **2**, 820–824.
8 M. Gliński, J. Kijeński and A. Jakubowski, *Appl. Catal., A*, 1995, **128**, 209–217.
9 O. Neunhoeffer and P. Paschke, *Ber. Dtsch. Chem. Ges.*, 1939, **72**, 919–929.
10 O. Nagashima, S. Sato, R. Takahashi and T. Sodesawa, *J. Mol. Catal. A: Chem.*, 2005, **227**, 231–239.
11 B. Boekaerts and B. F. Sels, *Appl. Catal., B*, 2020, **283**, 119607.
12 E. V. Fufachev, B. M. Weckhuysen and P. C. Bruijnincx, *ACS Sustainable Chem. Eng.*, 2020, **8**, 11292–11298.
13 Y. Yamada, M. Segawa, F. Sato, T. Kojima and S. Sato, *J. Mol. Catal. A: Chem.*, 2011, **346**, 79–86.
14 V. Yakerson, L. Lafer and A. Rubinshtein, *Bull. Acad. Sci. USSR, Div. Chem. Sci.*, 1966, **15**, 280–285.
15 R. Pestman, R. Koster, A. Van Duijne, J. Pieterse and V. Ponec, *J. Catal.*, 1997, **168**, 265–272.
16 C. A. Gaertner, J. C. Serrano-Ruiz, D. J. Braden and J. A. Dumesic, *J. Catal.*, 2009, **266**, 71–78.
17 H. Idriss and M. A. Barteau, in *Advances in Catalysis*, Elsevier, 2000, vol. 45, pp. 261–331.
18 T. N. Pham, D. Shi, T. Sooknoi and D. E. Resasco, *J. Catal.*, 2012, **295**, 169–178.
19 A. Gumidyala, T. Sooknoi and S. Crossley, *J. Catal.*, 2016, **340**, 76–84.
20 T. N. Pham, T. Sooknoi, S. P. Crossley and D. E. Resasco, *ACS Catal.*, 2013, **3**, 2456–2473.
21 B. Boekaerts and B. F. Sels, *Appl. Catal., B*, 2021, **283**, 119607.
22 A. Pulido, B. Oliver-Tomas, M. Renz, M. Boronat and A. Corma, *ChemSusChem*, 2013, **6**, 141–151.
23 J. T. Scanlon and D. E. Willis, *J. Chromatogr. Sci.*, 1985, **23**, 333–340.
24 K. Kim and M. Barteau, *J. Catal.*, 1990, **125**, 353–375.
25 S. D. Randery, J. S. Warren and K. M. Dooley, *Appl. Catal., A*, 2002, **226**, 265–280.
26 A. M. Jubb and H. C. Allen, *ACS Appl. Mater. Interfaces*, 2010, **2**, 2804–2812.
27 R. M. Cornell and U. Schwertmann, *The iron oxides: structure, properties, reactions, occurrences and uses*, John Wiley & Sons, 2003.
28 J. A. Bennett, C. M. Parlett, M. A. Isaacs, L. J. Durndell, L. Olivi, A. F. Lee and K. Wilson, *ChemCatChem*, 2017, **9**, 1648–1654.
29 F. G. E. Nogueira, J. H. Lopes, A. C. Silva, R. M. Lago, J. D. Fabris and L. C. A. Oliveira, *Appl. Clay Sci.*, 2011, **51**, 385–389.
30 M. J. Tiernan, P. A. Barnes and G. M. Parkes, *J. Phys. Chem. B*, 2001, **105**, 220–228.
31 W. K. Jozwiak, E. Kaczmarek, T. P. Maniecki, W. Ignaczak and W. Maniukiewicz, *Appl. Catal., A*, 2007, **326**, 17–27.
32 H.-Y. Lin, Y.-W. Chen and C. Li, *Thermochim. Acta*, 2003, **400**, 61–67.
33 T. Yamashita and P. Hayes, *Appl. Surf. Sci.*, 2008, **254**, 2441–2449.

34 A. A. Taimoor, A. Favre-Reguillon, L. Vanoye and I. Pitault, *Catal. Sci. Technol.*, 2012, **2**, 359–363.
35 E. Karimi, A. Gomez, S. W. Kycia and M. Schlaf, *Energy Fuels*, 2010, **24**, 2747–2757.
36 N. Mimura, I. Takahara, M. Saito, T. Hattori, K. Ohkuma and M. Ando, *Catal. Today*, 1998, **45**, 61–64.
37 T. S. Hendren and K. M. Dooley, *Catal. Today*, 2003, **85**, 333–351.
38 J. Kuriacose and S. Jewur, *J. Catal.*, 1977, **50**, 330–341.
39 A. V. Ignatchenko, *J. Phys. Chem. C*, 2011, **115**, 16012–16018.
40 K. M. Dooley, A. K. Bhat, C. P. Plaisance and A. D. Roy, *Appl. Catal., A*, 2007, **320**, 122–133.
41 D. Martin and D. Duprez, *J. Phys. Chem.*, 1996, **100**, 9429–9438.
42 T. Yamaguchi, *Catal. Today*, 1994, **20**, 199–217.
43 F. Fally, V. Perrichon, H. Vidal, J. Kaspar, G. Blanco, J. Pintado, S. Bernal, G. Colon, M. Daturi and J. Lavalley, *Catal. Today*, 2000, **59**, 373–386.